GPS APPLICATIONS FOR GEODYNAMICS AND EARTHQUAKE STUDIES

Paul Segall

Department of Geophysics, Stanford University, Stanford, California 94305;
e-mail: segall@geo.stanford.edu

James L. Davis

Harvard-Smithsonian Center for Astrophysics, 60 Garden Street, Cambridge,
Massachusetts 02138; e-mail: jdavis@cfa.harvard.edu

ABSTRACT

Geodetic measurements obtained with the Global Positioning System (GPS) are increasingly more widely applied in geophysical studies. In this paper, we review the changes to the technology of GPS geodesy over the last five years that are responsible for this increased applicability. We survey geophysical investigations employing GPS to measure coseismic, postseismic, and interseismic deformation; plate motion and crustal deformation at plate boundaries; volcano deformation; and the deformation associated with glacial isostatic adjustment and its application to sea-level studies. We emphasize the use of GPS determinations for the modeling of this wide variety of geophysical phenomena. We also discuss the recent advent of permanent GPS networks for regional geophysical studies, as well as the possible future of GPS surveying in light of the recent advances.

INTRODUCTION

The Global Positioning System (GPS), designed by the US Department of Defense for military and civilian navigation and positioning, has become the geodetic method of choice for studying a wide range of geophysical phenomena. GPS measurements are now in use to determine the motion of the Earth's tectonic plates, to study deformation around active faults and volcanos, and to measure the adjustment of the Earth's surface due to past and present changes in

301

the mass of the world's ice sheets. GPS is used in combination with tide gauges to monitor global changes in sea level. Because GPS signals are measurably delayed as they pass through the earth's atmosphere, GPS measurements are even able to contribute to atmospheric studies.

Several reasons contribute to the tremendous growth in GPS research. GPS provides three-dimensional relative positions with the precision of a few millimeters to approximately one centimeter over baseline separations of hundreds of meters to thousands of kilometers. The three-dimensional nature of GPS measurements allows one to determine vertical as well as horizontal displacement at the same time and place. Previously, horizontal measurements were often made by trilateration and vertical measurements by spirit leveling. The fact that the two data types were almost never collected at the same time and place complicated analysis considerably. Furthermore, vertical and horizontal information together often place more robust constraints on physical processes than do either data type alone. GPS receivers and antennas are portable, operate under essentially all atmospheric conditions, and do not require intervisibility between sites.

The primary reason for the growth in crustal deformation research with GPS, however, is the fact that the technique puts an inexpensive, precise geodetic tool in the hands of scores of university and other research groups. Unlike other space geodetic techniques, such as Very Long Baseline Interferometry (VLBI) and Satellite Laser Ranging (SLR), that require large facilities and budgets, GPS measurements can be collected by small teams with modest budgets. For this reason, GPS has essentially replaced mobile VLBI and SLR for the study of plate motions and plate boundary deformation. GPS has also largely replaced trilateration and, to a lesser degree, spirit leveling in the study of crustal deformation associated with earthquakes and volcanos. For example, the highly successful Crustal Strain Project of the US Geological Survey switched from a ground-based laser distance measuring device to GPS in the late 1980s.

Strainmeters still provide far greater strain sensitivity than does GPS, but they cannot offer the spatial coverage and long-term stability of GPS. Interferometric Synthetic Aperture Radar (SAR) measurements are tremendously exciting because of their unparalleled spatial coverage. Interferometric SAR and GPS are complementary in that GPS provides long-term stability, vector displacements, and better temporal coverage as compared to the extensive spatial coverage provided by SAR. Because both GPS and SAR (as well as VLBI) involve the propagation of electromagnetic signals, they share related path delays through the electrically neutral lower atmosphere. Thus, results from one system are directly relevant to the others, and presently strong interest exists in using GPS estimates of atmospheric water vapor to correct SAR images for the variable path delay induced by water vapor.

GPS has already had a significant impact on the earth sciences, and a large body of literature on the technique and results is available. Rather than attempt to comprehensively review this body of work, we focus here on representative results of recent (post-1991) solid earth studies employing GPS. We do not cover developments in the many other scientific applications of GPS, such as GPS meteorology. We begin by briefly reviewing changes in the technology and our understanding of error sources during the past five years.

SURVEYING WITH GPS: TECHNOLOGY

Although the GPS technique remains fundamentally the same as that described by Hager et al (1991) and Dixon (1991), many of the particulars have changed. [The reader is referred to these papers as well as to books by Hofmann-Wellenhof et al (1994), Leick (1995), and Parkinson et al (1996) for a thorough description of the GPS system.] The situation only five years ago, as described by Dixon (1991), consisted of 15 GPS satellites in orbit. Selective availability (SA) had been enabled, anti-spoofing (AS) had not. Satellite coverage limited the length of the observing session to 7–8 h per day, and most published work still relied on the four-satellite–maximum TI-4100 GPS receiver. The current situation is quite different now, as discussed below.

What is the demonstrated accuracy of GPS? Five years ago, a great deal of effort was focused on this question. Nearly every article included a plot of (usually horizontal) repeatabilities of site position vs baseline length. Repeatability is usually defined to be the root mean square (rms) residual about the best-fit straight line. The translation from "repeatability" to "accuracy" is not straightforward. For example, GPS and VLBI determinations have never really agreed at a level better than 10 mm or so (e.g. Larson & Agnew 1991). Since the early 1990s, publications have tended to focus on specific subjects, examples of which are orbits (e.g. Beutler et al 1996; Fliegel et al 1992), effects of precipitation (e.g. Tranquilla & Al-Rizzo 1993) and snow accumulation (e.g. Jaldehag et al 1996), and atmospheric pressure loading (e.g. vanDam et al 1994). (This latter is an "error" only insofar as it is ignored in the models for time-dependent station position.) Heflin et al (1992), with a still-incomplete satellite constellation, reported a short-term (three week) rms misfit σ about the weighted mean, which varied linearly with baseline length L

$$\sigma = a + bL, \tag{1}$$

with $a = 2$ mm and $b = 4$ parts-per-billion (ppb), for baselines in the northern hemisphere with $L < 12{,}000$ km. (Other forms for σ have been used in the literature, including $\sigma^2 = a^2 + b^2 L^2$.) More recently, Jaldehag (1995) reported on long-term (two year) repeatability from the Swedish permanent GPS network
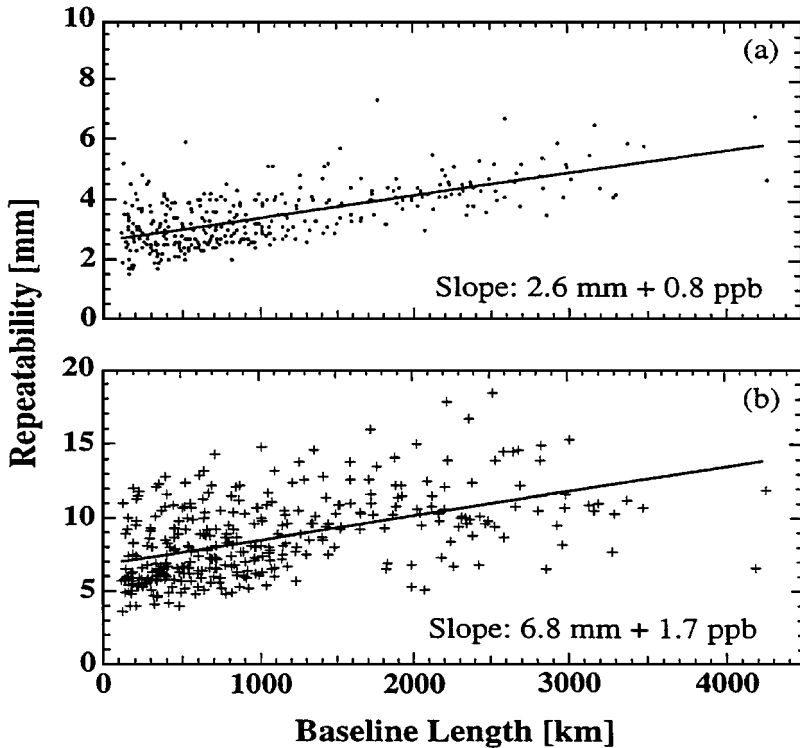
Figure 1 Weighted rms misfit about the best fit line for (a) baseline length and (b) vertical component of the baseline vector, for the 21-site Swedish permanent GPS network (Jaldehag 1995). Included in the analysis were several European sites of the International GPS Service for Geodynamics (IGS).

and found, for the horizontal, $a = 2.6$ mm and $b = 0.8$ ppb, and, for the vertical, $a = 6.8$ mm and $b = 1.7$ ppb, for baselines up to $\sim$4000 km (Figure 1). Assuming that the differences between the GPS and VLBI determinations lie either with the VLBI system or the tie between reference points, then it seems clear that individual GPS measurements across regional scales have accuracies of $\sim$2–5 mm for the horizontal components and are a factor of 3 worse for the vertical components.

Note that these conclusions are for "permanent" GPS networks. Campaign-style measurements are inevitably less precise owing to errors in centering the GPS antenna and measuring its height over the benchmark. Precision in daily position determinations decrease, although slowly, as the length of observing sessions decreases from 24 h. Longer observing sessions tend to average out

signal multipath (see below), and offer improved ambiguity resolution and estimation of atmospheric delays. So-called rapid-static (e.g. Merminod & Rizos 1994) or kinematic (e.g. Lu & Lachapelle 1992) methods have achieved centimeter-level horizontal precision on short to intermediate baselines.

In the remainder of this section, we focus on four areas that have evolved significantly in the last several years. These areas are (*a*) the GPS constellation, including the impact of broadcast signal degradation and encryption; (*b*) GPS receivers and antennas, with a discussion of errors caused by antenna phase-center variations, multipath, and electromagnetic coupling; (*c*) available global infrastructure for GPS geodesy; and (*d*) atmospheric propagation delay, one of the most important sources of error in the analysis of GPS data. Of course, this is far from an exhaustive list of all issues relevant to the technology of GPS surveying. Blewitt (1993), for example, discusses ambiguity resolution, treatment of clock errors, and surveying methods, and because of the important changes to GPS in the last several years, all these topics could be revisited here. Instead, our treatment is limited to several important topics, and the discussion of the detailed implications for GPS surveying methods and technology can be found in the cited works.

The GPS Constellation

The 24-satellite GPS network was first realized in July 1992. It is difficult to overestimate the impact that the increased satellite coverage has had, not only on logistical planning for a measurement campaign, but also on the accuracy achievable in parameter estimates (e.g. Santerre 1991) and, ultimately, on the kinds of science to which it is possible to apply GPS. For example, continuous satellite coverage enables subdaily, continuous estimation of position (Genrich & Bock 1992; Elósegui et al 1996) and atmospheric water vapor and temperature (e.g. Yuan et al 1993; Rocken et al 1995). The improved geometric coverage globally has also enabled the development of "fiducial-free" network solutions (e.g. Heflin et al 1992).

The related issues of selective availability (SA) and anti-spoofing (AS) continue to be concerns in geodetic applications. Both SA and AS were implemented for US national security reasons, and both limit the accuracy of the GPS technique for certain applications. SA degrades the quality of the broadcast satellite position information and clock corrections, as well as the effective satellite oscillator frequency. This "dithering" introduces noise to the measured carrier beat phases, with changes in the transmitted L1 frequency, for example, of up to 1 Hz (Feigl et al 1991). Several schemes have been developed for dealing with this aspect of SA (e.g. Feigl et al 1991; Rocken & Meertens 1991). For geodetic applications in which double-differencing (or its equivalent) can be applied to synchronized observations (e.g. Hofmann-Wellenhof et al 1994),

the effect of SA is nearly negligible (Rocken & Meertens 1991). The stated policy of the US government is to discontinue the use of SA "within the next decade" (Office of Science Technology Policy 1996).

AS involves the encryption of the precise code (P-code). The coarse acquisition code (C/A) is still available when AS is enabled. Many of the early high-precision GPS receivers required acquisition of the P-code. One of the initial responses to AS was the development of "squaring" receivers, which provided C/A code pseudoranges (on the L1 channel only) and half-wavelength L2 carrier phases. Halving the wavelength, however, makes resolution of integer phase ambiguities much more difficult. More recently, manufacturers have adopted a variety of methods for delivering full wavelength L2 phase data as well as dual frequency pseudorange, even in the presence of AS (e.g. Hofmann-Wellenhof et al 1994). The observables obtained in periods of AS are somewhat noisier, with a degradation of the signal-to-noise ratio of 14–30 dB, depending on the method used (Hofmann-Wellenhof et al 1994). This degradation has a cascading effect greater than that suggested by the propagation of larger phase uncertainties, because these increased uncertainties hinder the elimination of phase ambiguities from the solution.

GPS Receivers and Antennas for Geodesy

Blewitt (1993) reviewed the development of GPS receivers from the early 1970s to the early 1990s. Since that publication, a great number of commercial GPS receivers have gone on the market. One of the most significant of recent changes has been the cost of GPS receivers. As of this writing, geodetic quality GPS receivers cost $15,000 or less if bought in quantity, a decrease of ~50% in about five years. (In the mid-late 1980s, an equivalent GPS receiver cost ~$200,000.) This decrease in cost has had an enormous impact, enabling a very large global network of permanent sites to be established, thereby increasing the accuracy of the satellite orbit determinations. The low cost also allows a greater number of groups to become involved, increasing the variety of science that is being addressed. GPS projects now typically involve a greater number of GPS receivers, which enables a greater density of sites, improving spatial resolution and easing logistics. Finally, GPS receivers may now be dedicated to a project, enabling a growth of so-called "continuous GPS" (or "permanent GPS") (see below).

The latest generation of GPS receivers has several practical features that make them far superior in the field to receivers available even a few years ago. Receivers having eight or more physical dual-frequency channels are now available, allowing all satellites in view to be tracked simultaneously. The receivers are very light, usually under 4 kg, and consume 12 W or less power. Data from several days can be stored in nonvolatile RAM.

An important component of ground-based GPS receiving systems that heretofore received relatively little attention (from geophysicists) has been the antenna.

To simplify ground-based GPS receiving systems, and to reduce costs and improve portability, GPS receiving systems have been designed to use antennas that accept signals arriving from all directions. The ground-plane is designed to reduce the effects of signals received from negative elevation angles, but such signals are not rejected completely. These signals, reflected from nearby objects, interfere with the "direct" signal, causing a phase error known as multipath. For example, the ground, which can be modeled as an infinite planar reflector, causes multipath that varies sinusoidally with elevation angle of the satellite and thus nearly averages out over sufficiently long periods of time (e.g. Elósegui et al 1995). (The period of ground-based multipath oscillation, in hours, is of order (λ/H), where λ is the L1 or L2 wavelength and H the height above the ground.)

Objects placed very close to the antenna actually become electromagnetically coupled to the antenna system, effectively modifying the antenna phase pattern (the variation of received phase with direction) (e.g. Krauss 1988). These phase patterns, even for an isolated antenna system, are difficult to characterize analytically (e.g. Wu et al 1993). Schupler et al (1994) measured in an anechoic chamber the electrical properties of several different models of geodetic GPS antennas. They found large (20–40°) variations of phase with direction and significant differences between the patterns of antennas of different design. The problem is compounded when nearby objects become coupled to the antenna. Elósegui et al (1995) found that the electromagnetic coupling between the GPS antenna and the pillar on which it is mounted can cause large phase errors that, unlike multipath, do not average out. One implication of this problem is that antennas of identical design, but mounted in the field differently, have different effective phase patterns.

Infrastructure for GPS Geodesy

A large permanent infrastructure supporting GPS geodesy has, in many ways, revolutionized how geodetic observations are planned, acquired, and analyzed. The International GPS Service for Geodynamics (IGS), which formally became operational on January 1, 1994, is composed of a global network of permanent GPS stations, data centers, analysis centers, a central bureau, and a governing board (e.g. Beutler et al 1993; Zumberge et al 1995). The "IGS network" is presently composed of nearly 100 GPS stations. Each permanent site is operated independently by its parent institution, and the network links are provided by the Internet. The principal products of the IGS analysis centers are routinely available within several days after aquisition, and include the following: high-accuracy GPS ephemerides (orbits), Earth rotation parameters, satellite and station clock information, and ionospheric information.

Investigators may count on the availability of nearby IGS sites, with well-measured velocities, to densify campaign-style regional GPS surveys and to

obtain an accurate tie to a global terrestrial reference frame, such as the International Terrestrial Reference Frame (ITRF) of the International Earth Rotation Service (IERS) (see http://hpvlbi.obspm.fr/iers/ierscb.html). Investigators may use data from a global subnetwork of choice to estimate satellite ephemerides, or they may utilize the IGS ephemerides provided by the analysis centers. Whereas in the past GPS analysts often spent a great amount of time acquiring and "cleaning" tracking data for the determination of satellite orbits, they can now simply download high precision ephemerides from the Internet. The availability of a global data set means also that global geophysical studies, such as plate motion studies reviewed below, and even some regional studies, can be undertaken for the cost of data analysis only.

Atmospheric Propagation

The atmosphere slows the propagation of the GPS signals, thereby increasing the observed phase. The neutral atmosphere, unlike the ionosphere, is not dispersive at GPS carrier frequencies, so that estimates of site position (in particular the vertical coordinate) are sensitive to atmospheric modeling errors. In GPS studies, the atmospheric propagation delay τ_a is often expressed as the sum of two terms

$$\tau_a(\epsilon) = \tau_h^z m_h(\epsilon) + \tau_v^z m_v(\epsilon), \tag{2}$$

where τ_a is taken to be dependent on elevation angle ϵ but not on azimuth. The first term (with subscript h) represents the hydrostatic delay; the second term (subscript v) represents the water-vapor or "wet" delay (Davis et al 1985). Each of the two terms is the product of two quantities: the zenith delay (superscript z) and the "mapping function," which maps the delay at zenith to lower elevations. The total atmospheric delay at zenith is about 2.4 m.

Typically, the mapping functions are assumed to be known. Because water vapor can vary at altitude, the zenith wet delay τ_v^z cannot accurately be estimated using surface measurements only. Although the hydrostatic zenith delay can be accurately estimated from surface pressure, this information is often not available, and a nominal value for surface pressure is used. The remaining unknown delay, $\Delta\tau_a$, thus depends on $\Delta\tau_h^z$, the difference between the true hydrostatic zenith delay and the nominal value used. The approximation that $m_h(\epsilon) \simeq m_v(\epsilon)$ enables $\Delta\tau_a$ to be written as

$$\Delta\tau_a \simeq \left(\Delta\tau_h^z + \tau_v^z\right)m_v(\epsilon). \tag{3}$$

The combined zenith-delay correction $(\Delta\tau_h^z + \tau_v^z)$ is then estimated in the GPS phase solution, along with site positions and other parameters. The error in Equation 3 is $\Delta\tau_h^z \Delta m(\epsilon)$, where $\Delta m(\epsilon)$ is the difference between the hydrostatic and wet mapping functions. Using the mapping functions of Niell (1996),

the average difference between the hydrostatic and wet mapping functions for a latitude of $45°$ is 4 mm for $\epsilon = 20°$ and 30 mm for $\epsilon = 10°$ ($\Delta\tau_h^z = 300$ mm). This error is an effective mapping-function error that has the potential to bias site position estimates (e.g. Davis et al 1991). Thus, the error in the a priori zenith delay should be as small as possible.

Although errors in the mapping functions could have significant effects on site parameter estimates (Davis et al 1985), these errors are small for recently developed mapping functions. Niell (1996) reported that estimated lengths of baselines varied by less than 5 mm as the elevation cutoff angle was reduced from $12°$ to $3°$, for baselines longer than 10,000 km. Given that most GPS analyses do not use data below $15°$, we can conclude that mapping function errors are generally negligible (but see below).

Estimation of zenith delays from GPS data significantly weakens the solutions owing to the correlations between these parameters and the vertical site coordinates. Independent estimates of wet delay from ground-based water-vapor radiometers (WVRs) (e.g. Elgered et al 1991) therefore continue to attract considerable attention. The accuracy of the WVR technique depends both on the WVR instrumental calibration and on the algorithm that uses the measured atmospheric brightness temperatures to estimate the wet delay. Although some improvements have been made in techniques for instrumental calibration, comparisons of side-by-side WVRs reveal rms differences of $\sim$2–6 mm (e.g. Kuehn et al 1993; Ware et al 1993). Although much improvement has been obtained in WVR algorithms (e.g. Johansson et al 1993), until laboratory measurements improve the accuracy of the attenuation coefficient and refractive index of water vapor, it is doubtful that wet delay values estimated from WVR data can exceed the 4–6% level in accuracy (Elgered et al 1991).

A potentially more serious problem is that mapping functions are usually assumed to be azimuthally symmetric. This idealization of the atmosphere can lead to significant errors in the mapping function. Sinusoidal azimuthal variations in the atmospheric propagation delay have been determined from VLBI data (e.g. MacMillan 1995) and from WVR data (e.g. Rocken et al 1991; Davis et al 1993). Sinusoidal variations with amplitudes as large as 8 cm at $20°$ elevation have been observed (Davis et al 1993). Azimuthal mapping function errors have a potentially significant effect on the estimates of site position from GPS data, but there have been few studies quantitatively assessing this effect.

GPS AND EARTHQUAKE STUDIES

As discussed in the introduction, GPS has become the geodetic method of choice for studying deformation associated with earthquakes. Before describing some results obtained with GPS, we first address the more general role of crustal
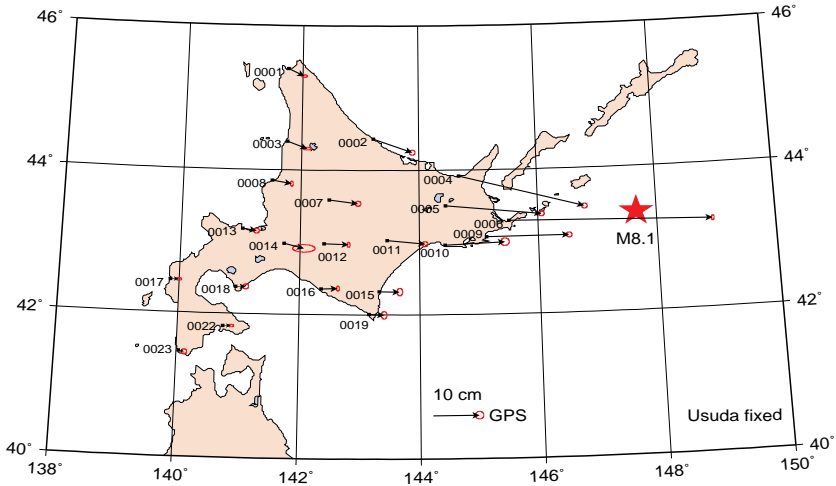
Figure 2 Horizontal displacement vectors from the M8.1 Kurile Islands (Hokkaido-Toho-Oki), Japan, earthquake, October 4, 1994. Displacements are relative to a station 1100 km away. Error ellipses show 99% confidence regions. After Tsuji et al (1995).

deformation measurements in the study of earthquakes. These measurements are complementary to seismological data because they document the full earth-quake cycle, including interseismic and transient postseismic processes, as well as coseismic deformation. Detection of slow interseismic strain accumulation is probably the best technique we have for identifying the location of future earthquakes in some areas, because elastic rebound requires elastic strain ac-cumulation prior to earthquakes. Postseismic strain relaxation is important in constraining transient stress transfer and may provide insight into physical pro-cesses active on faults. For these reasons, measurement is essential of both the quasi-static deformations associated with faulting and the dynamically radiated seismic waves.

Coseismic Deformation

Coseismic displacements (e.g. Figure 2) have been determined with GPS for at least 15 recent earthquakes (Table 1). Although this table is likely to be incomplete, certainly by the time of publication, it does give a feeling for the number and kind of earthquakes for which GPS data have been collected.

GPS measurements can be related to the earthquake source process through Volterra's formula (e.g. Aki & Richards 1980) for displacement at the Earth's surface due to slip on a surface of displacement discontinuity in an elastic medium. GPS measurements of surface displacement can thus be inverted to determine the geometry of earthquake rupture(s). This determination is

Table 1   Recent earthquakes for which coseismic displacements have been determined by GPS

Earthquake	Magnitude (M)	References
1987 Superstition Hills, California	6.2	Larsen et al 1992
1989 Loma Prieta, California	7.1	Lisowski et al 1990, Williams et al 1993
1989 Kalapana, Hawaii	6.1	Dvorak 1994
1991 Valle de la Estrella, Costa Rica	7.7	Lundgren et al 1993
1992 Cape Mendocino, California	7.0	Murray et al 1996
1992 Joshua Tree, California	6.1	Bennett et al 1995
1992 Landers, California	7.3	Blewitt et al 1993, Bock et al 1993, Hudnut et al 1994, Freymueller et al 1994
1993 Guam	7.8	Beavan 1993
1994 Northridge, California	6.7	Hudnut et al 1996, Shen et al 1996
1994 Arthurs Pass, New Zealand	6.7	Árnadóttir et al 1995
1994 Hokkaido-Toho-Oki, Japan	8.1	Tsuji et al 1995
1994 Sanriku-Haruka-Oki, Japan	7.5	Miyazaki et al 1996
1995 Hyogo-ken Nanbu (Kobe), Japan	7.2	Tabei et al 1996
1995 Anatofagasta, Chile	8.1	Ruegg et al 1996
1995 Jalisco, Mexico	8.0	Melbourne et al 1996

particularly important for earthquakes that do not rupture the ground surface, or when seismic data, including aftershock distributions, do not clearly determine the rupture geometry.

In estimating the source geometry, an earthquake is typically represented by one or more rectangular dislocations with spatially uniform slip. Once the fault geometry is known, it is possible to determine the distribution of slip on the fault surface, as discussed below. Estimation of the finite source geometry from observed displacements at the Earth's surface is a discrete nonlinear optimization problem. In the past few years, a number of groups have used numerical optimization procedures to determine the best-fitting dislocation surface or surfaces. The methods can generally be divided into two categories: those methods, such as nonlinear least squares or quasi-Newton methods, that make explicit use of the first or second derivatives and Monte Carlo methods that do not require these derivatives.

Several recent earthquakes have occurred in areas of sufficiently good GPS-site coverage to allow the fault geometry to be estimated solely from geodetic observations. We summarize here results for the 1989 Loma Prieta, 1992 Cape Mendocino, and 1994 Northridge earthquakes. One might reasonably wonder

why such efforts are required, given that considerable information about source geometry is obtained from seismic data and direct observation of fault ruptures. The answer is twofold: First, seismic and geologic data often do not completely constrain the fault geometry. In all three cases considered here, primary fault rupture did not reach the Earth's surface. In addition, aftershock distributions can be complex, with substantial activity off the principal fault surface. Thus, geodetic observations can play a substantial role in elucidating the geometry of the fault rupture. The second reason is that analysis of coseismic deformation serves as a testing ground for the development of methods, which can then be applied to the more challenging problem of imaging the sources of post-seismic and interseismic strain. Postseismic and interseismic deformations are much smaller than coseismic deformations, and there is little or no supporting information from seismic measurements.

Árnadóttir & Segall (1994) used all available geodetic data, including GPS measurements, to determine the geometry and slip distribution in the 1989 Loma Prieta earthquake. They used a quasi-Newton method to solve the optimization problem and a bootstrap procedure to estimate confidence intervals in the derived parameters. The location and orientation of the inferred Loma Prieta dislocation surface are consistent with well-located aftershocks, with most of the aftershocks occurring slightly deeper than the inferred dislocation. In contrast, some earlier results had found the best-fitting dislocation to be offset by up to 2 km from the aftershock zone. Bootstrap calculations of the confidence intervals showed that the slight offset between the center of the aftershock zone and the inferred rupture was well within uncertainties (Árnadóttir & Segall 1994).

For the M7 1992 Mendocino earthquake, Murray et al (1996) used a combination of GPS-derived displacements, spirit-leveling measurements, and coastal uplift determined by the death of intertidal marine organisms to estimate the geometry of the rupture surface. They used a random search procedure that selects candidate models over some (nonuniformly spaced) grid in model space. The best-fitting dislocation has dip, location, and sense of slip consistent with a subduction zone event, making it the first well-documented earthquake to occur on the Cascadia mega-thrust. Results of the geodetic inversion are generally consistent with seismic results; however, the estimated dislocation surface dips more steeply than either the long period nodal plane or the band of aftershocks. The best-fitting dislocation surface is also somewhat shallower than the aftershock zone, although the resolution of the geodetic data is such that a dislocation surface within the aftershock zone could not be rejected.

The M6.7 January 1994 Northridge earthquake was possibly the best geodetically monitored earthquake yet to occur. Vector displacements were determined at 66 GPS sites (Hudnut et al 1996). Hudnut et al (1996) used the random cost
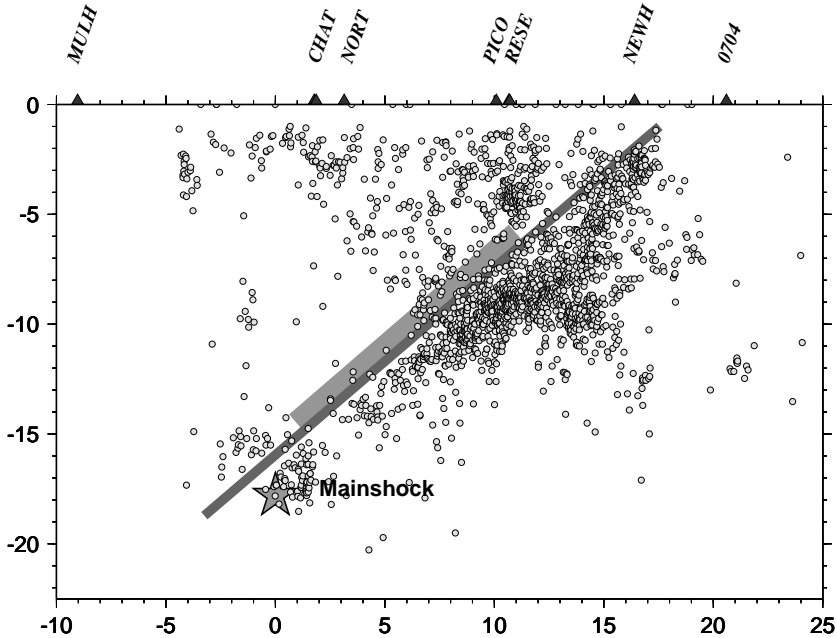
Figure 3 Cross section through the 1994 Northridge earthquake, showing relocated aftershocks and the uniform slip dislocation inferred from modeling of GPS displacements (*thick line*). Also shown is the extended dislocation plane used to model the spatial variation in slip (*thin line*). After Hudnut et al (1996).

method and found that the best-fitting rectangular dislocation does not pass through the principal concentration of aftershocks, but is displaced 1–2 km into the hanging wall (Figure 3). These authors note that a model with a single dislocation surface does not fit the GPS data satisfactorily. Shen et al (1996) analyzed the same data set using an iterative search procedure. They also found that the data cannot be well fit by a single dislocation extending through the mainshock and concentrated zone of aftershocks. By including a more steeply dipping shallow up-dip extension of the main rupture (a "hinged" fault) as well as a secondary antithetic fault located northwest and above the main shock, these authors arrive at a satisfactory fit to the data. Support for deformation northwest of the mainshock comes from interferometric SAR results (Massonet et al 1996).

The systematic tendency of these geodetically inferred dislocation surfaces to be shallower than the corresponding aftershock zones has been observed for a number of other earthquakes. A number of factors probably contribute:

systematic mislocation of aftershocks due to three-dimensional velocity variations, bias in the geodetic estimates due to elastic inhomogeneity, and nonplanar fault geometry. Failure to account for elastic inhomogeneity systematically biases geodetic inversions to shallow fault depths. The quality and quantity of geodetic observations have increased so dramatically in the last decade that it now seems probable that the effects of inhomogeneity, and perhaps anisotropy, in the Earth's crust can no longer be neglected (e.g. Du et al 1994).

If the geometry of the fault surface is known, then GPS observations of surface displacement can be inverted for the spatial distribution of fault slip using linear inverse methods. Although the information in slip estimates is fundamentally kinematic, the estimates do provide important observational constraints on mechanics of the earthquake process. To circumvent the inherent nonuniqueness in the inversion, the problem can be regularized by seeking slip distributions that simultaneously fit the data to an acceptable degree and satisfy some a priori criterion, such as smoothness (e.g. Matthews & Segall 1993). The appropriate tradeoff between data fit and solution roughness can be quantitatively determined using cross validation (Matthews & Segall 1993). Simulations show that cross validation yields optimal estimates of the smoothing parameter for a given model norm if data correlations are properly accounted for (Árnadóttir & Segall 1994). It is reasonable to assume that the fault slip does not change direction on the fault surface, in which case a non-negativity constraint is imposed on the solution.

Geodetic estimates of slip distribution complement seismic data in elucidating the earthquake rupture process. The radiated seismic wave field is dependent on the slip amplitude, rupture velocity, and source time function, whereas the quasistatic displacements depend only on the final slip amplitude. Therefore, a combination of seismic and geodetic data provides stronger constraints on the spatial distribution of slip and the temporal evolution of rupture than do seismic data alone (e.g. Cohee & Beroza 1994). Whereas static slip distributions have been estimated for a number of earthquakes using geodetic observations (e.g. Larsen et al 1992; Bennett et al 1995), in the last few years emphasis has been on combined inversion of seismic and geodetic data. We review here results for recent California earthquakes. Yoshida et al (1996) presented a combined geodetic and seismic inversion in their study of the Hyogo-ken Nanbu, Japan (Kobe), earthquake.

The estimated slip distribution in the 1989 Loma Prieta earthquake agrees reasonably well with inversions of strong motion seismic data (Árnadóttir & Segall 1994). Using cross validation to estimate the smoothing parameter, the slip is found to be more localized than that obtained in seismic inversions. At present, it is not known whether this difference is due to neglected correlations in the data, which bias cross validation toward rough models, or whether subjective

methods used to determine the amount of smoothing in the seismic inversions tend to overly smooth the slip distribution.

Extensive data from permanent GPS (Blewitt et al 1993; Bock et al 1993), survey GPS (Hudnut et al 1994), and geodimeter networks allowed the static-slip distribution to be computed for the M7.3 Landers earthquake. Although the precise slip distribution cannot be uniquely resolved, Johnson et al (1994) were able to find a strict lower bound on the seismic moment using the GPS observations. Slip estimates obtained from geodetic observations (e.g. Freymueller et al 1994) indicate two major slip patches, in agreement with inversions of seismic data. As with the Loma Prieta earthquake, cross validation leads to estimates that are substantially more localized with greater plate slip (Freymueller et al 1994) than those obtained from inversion of seismic data (Cohee & Beroza 1994; Wald & Heaton 1994). In addition to the factors discussed above, mismodeling of the complex rupture geometry in this earthquake could bias cross validation, particularly for stations very near to the fault.

Wald & Heaton (1994) included geodetic, teleseismic, and strong motion data in their analysis of the Landers earthquake. Given a consistent fault geometry and discretization, they are able to compare models obtained independently from each data set. Inclusion of permanent displacements and the near field seismic data should result in improved estimates of slip and rupture velocity in the earthquake. As Cohee & Beroza (1994) point out, however, assigning appropriate weights to the geodetic and seismic data is complicated by the fact that in the seismic case, errors are dominated by inaccuracy in the calculation of synthetic seismograms rather than by measurement error.

For the 1994 Northridge earthquake, Wald et al (1996) analyzed a combination of seismic (teleseismic and strong motion) and geodetic (GPS and leveling) data to determine the slip distribution and rupture history of the Northridge earthquake. In this case, inversions conducted with the various data sets do not agree well with one another. The geodetic data can be fitted reasonably with a very smooth slip distribution that is inconsistent with the strong-motion data. This inconsistency emphasizes the poor resolution of geodetic data for relatively small and deep earthquakes.

Postseismic Deformation

GPS will play an increasingly important role in improving our knowledge of postseismic processes. Traditional seismic instruments are insensitive to postseismic processes, with the exception of aftershocks. Strainmeters and tiltmeters record short-term transients following earthquakes, but only geodetic survey measurements are likely to have the spatial coverage and long-term stability needed to resolve postseismic strains with characteristic times of years to decades. Prior to the advent of GPS, very few postseismic data sets existed for

comparison to theoretical predictions. It will be some time before decade-long GPS data sets have been collected that follow a significant number of large earthquakes. Nevertheless, given the precision of the measurements and the relative ease of GPS surveying, we can expect a revolution in our understanding of postseismic processes in the upcoming decade. In the last three years alone, five earthquakes of M7.5 and greater have occurred within existing GPS networks (Table 1).

Because they were among the first major earthquakes to be well recorded using GPS, the 1989 Loma Prieta and 1992 Landers earthquakes are the first to yield significant postseismic strain signals. Following the Loma Prieta earthquake, Savage et al (1994) found evidence for a decaying transient with a characteristic time of ∼1.4 years, from the first 3.3 years of data. Interestingly, the transient is most clearly expressed in the component of motion perpendicular to the San Andreas fault; the fault parallel component exhibits little evidence of a decaying transient. Bürgmann et al (1996), when analyzing this and additional data, used a model of San Francisco Bay area deformation to remove the expected effects of interseismic deformation from the data. The residual postseismic velocities are significantly nonzero only within about 20 km of the rupture zone, effectively limiting the source of postseismic deformation to the seismogenic upper crust. Deformation at greater depths, including distributed asthenospheric flow, would generate more widely distributed deformation at the Earth's surface.

The residual postseismic motions include contraction normal to the trend of the San Andreas, particularly on the northeast footwall side of the fault, as well as accelerated right-lateral deformation. Savage et al (1994) modeled the postseismic deformation with oblique slip on a 5-km wide down-dip extension of the coseismic rupture, as well as fault collapse on the coseismic rupture. They presumed the latter to be a reversal of dilatancy that occurred during the earthquake. Bürgmann et al (1996) used numerical optimization methods to show that the data are best fit by a combination of aseismic oblique-reverse slip on the Loma Prieta rupture zone and reverse slip on southwest-dipping thrust northeast of the San Andreas fault zone. The thrust found by the inversion lies near a zone of thrust faults northeast of the San Andreas, which have been active in the Holocene. Models with secondary thrusting offer a comparable fit to the GPS data and a substantially improved fit to precise leveling data in the area when compared to the fault collapse interpretation.

Extensive GPS monitoring was conducted following the 1992 Landers earthquake. Shen et al (1994) found a decaying transient with a characteristic time of ∼1 month in the first 6 months after the earthquake. Savage & Svarc (1996) found a decay time of 84 ± 23 days, superimposed on a linear trend from 3.4 years of data across the Camp Rock–Emerson segment of the Landers

Rupture. Savage & Svarc (1996) argued that the linear trends indicate deformation rates that are substantially faster than those observed prior to the earthquake, which thus reflect a longer term relaxation with a time scale of at least 5 years.

Shen et al (1994) concluded that postseismic slip was concentrated below the southern half of the coseismic rupture on the southern Johnson Valley and Eureka Peak faults. They also inferred slip at depth below the Banning segment of the San Andreas fault, raising concerns at the time about triggered slip on the San Andreas and underscoring the importance of postseismic deformation monitoring for short-term hazard evaluation. In contrast, Savage & Svarc (1996) found the greatest postseismic slip beneath the northern Camp Rock–Emerson segment of the rupture. They also found fault collapse beneath the Homestead Valley segment and fault extension (dilatancy) beneath the southern Johnson Valley segment. A synthesis of the various data sets, including interferometric SAR images, could help clarify competing interpretations of postseismic deformation.

The proliferation of continuous GPS networks means that we can also look forward to the ability to resolve rapid postseismic signals, which were previously only measurable with strain and tilt meters. A striking example of this is offered by the Japanese national GPS array, which recorded a transient following the Sanriku-Haruka-Oki earthquake (Figure 4).

Interseismic Deformation

Many of the early studies of interseismic deformation using GPS took place in southern California. These studies were also instrumental in developing geodetic GPS methods and in characterizing the precision and accuracy of the technique (e.g. Larson & Agnew 1991; Feigl et al 1993). Feigl et al (1993) presented a comprehensive review of GPS data collected in central and southern California between 1986 and 1992, as well as VLBI data collected between 1984 and 1991. They also discussed methods for obtaining and combining highly precise GPS solutions for the determination of station velocities in regional-scale networks. Daily solutions with phase ambiguities fixed to integers (where possible) were estimated with very loose constraints on the station coordinates. The loosely constrained solutions (positions, covariances, and satellite states), along with comparable VLBI solutions, were then combined a posteriori to determine station coordinates at some reference time and velocities. Different solutions were obtained to define a terrestrial reference frame, to determine station coordinates sufficiently accurately for ambiguity resolution, and finally to determine the best estimate of station velocities. This approach minimized, to the degree possible at that time, the effects of incorrect specification of fiducial station coordinates (see also Larson et al 1991).
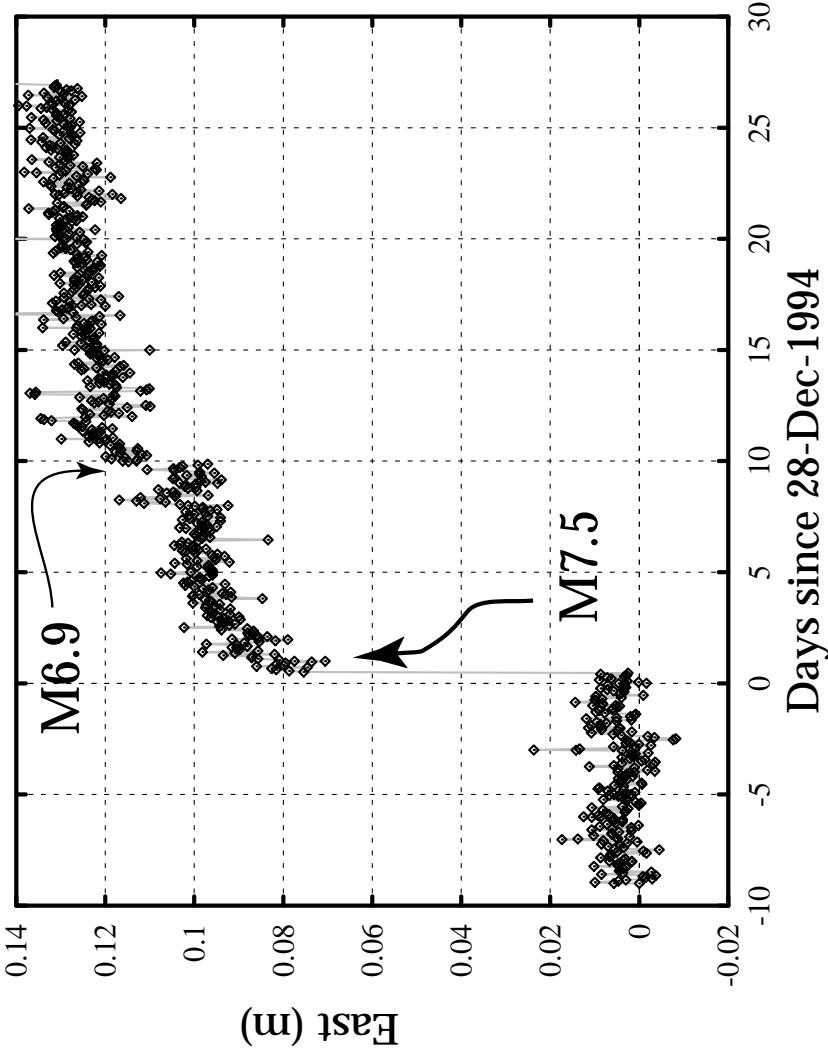
Figure 4 Postseismic deformation following the M7.5 Sanriku-Haruka-Oki, Japan, earthquake. Shown are estimates of the east component of displacement of station Kuji on the east coast of Honshu, Japan, determined every 75 min using data from the Japanese permanent GPS network. Note that the postseismic displacement is 25–40% of the coseismic signal. The north component shows a considerably smaller (<2 cm) transient. (F Webb, unpublished data.)

Feigl et al (1993) determined velocities for ~40 sites in central California with horizontal uncertainties of 2–3 mm/year. The most prominent feature of the data is right-lateral shear associated with North America–Pacific relative plate motion. Within uncertainties, the site at Vandenburg Air Force Base on the central California coast appears to be moving at the predicted velocity of the Pacific plate, although the data do allow several millimeters per year of offshore motion. San Clemente and San Nicolas Islands, off the coast near San Diego, also appear to move with Pacific plate velocity, whereas 6 ± 2 mm/year of motion between the islands and the mainland could be explained by offshore strike-slip faulting (Larson 1993).

In addition to strike-slip deformation, the GPS data reveal significant crustal shortening across the Santa Barbara Channel, the Ventura Basin, the Los Angeles Basin, and the Santa Maria fold and thrust belt (Feigl et al 1993). Although active folding and thrusting parallel to the San Andreas have long been known, and have generated damaging earthquakes including the 1983 Coalinga and 1985 Kettleman Hills earthquakes, detecting this shortening geodetically has been difficult. Feigl et al (1993) found 5.7 ± 0.5 mm/year of fault normal convergence between the California coastline and Owens Valley, which thus bounds the amount of shortening associated with individual structures across this broad region. These authors also find 5 ± 1 mm/year of shortening across the Los Angeles Basin between Palos Verdes and a site in Pasadena at the foot of the San Gabriel Mountains, which is consistent with geologic estimates.

GPS data show 6 ± 1 mm/year of roughly north-south convergence across the eastern Santa Barbara Channel (Larson 1993), which is consistent with both the geology and current seismicity of the region. This deformation continues on land into the Ventura Basin, where shortening is occurring at a rate of 7–10 mm/year, with strain-rates as large as 0.6 ± 0.1 microstrain/year (Donnellan et al 1993). The motion south of the Ventura Basin can be described by clockwise rotation of a rigid block at a rate of 8°/million years. The rate of shortening observed by GPS is a factor of two less than the geologic rate over the last 0.2 million years, but is consistent with the geologic rate over the last 1 million years. Donnellan et al (1993) conclude that the basin bounding faults must be slipping aseismically below depths of ~5 km, but that the upper locked segments could fail in earthquakes as large as M ~ 6.4. An eastern extension of these structures did rupture in the M6.7 Northridge earthquake, although to considerably greater depth than inferred from the GPS observations.

Bennett et al (1996) used additional GPS data through 1995 to investigate further the distribution of deformation across this plate boundary. Their estimate of 49 ± 3 mm/year for the North America–Pacific relative plate motion is consistent with previous space geodetic and geological plate rate estimates. They estimate slip rates for the southern San Andreas, San Jacinto, Elsinore,

Imperial, and Cerro Prieto faults of 26 ± 2, 9 ± 2, 6 ± 2, 35 ± 2, and 42 ± 2 mm/year, respectively. Other faults accomodating the remainder of the relative plate motion were inferred to lie to the west of the Elsinore fault. The authors concluded that off-fault strain accumulation is largely elastic and, on this basis, estimate the slip deficit accumulated on the southern San Andreas since its last rupture (ca 1680) to be over 8 m.

Subduction zones, as the loci of the world's largest earthquakes, are the focus of numerous GPS investigations. GPS studies in the Shumagin Islands, Alaska (Larson & Lisowski 1994), confirm earlier results showing that strain accumulation rates are an order of magnitude less than predicted by fully coupled dislocation models. In the Cascade subduction zone, three continuous GPS receivers have been in operation since 1992. The data show that Victoria (on the southern end of Vancouver Island) is moving 7 mm/year ENE relative to the presumed-stable North America plate (Dragert & Hyndman 1995). This together with leveling and tide gauge data are consistent with a 100-km wide section of the plate interface that is completely locked and a 100-km wide partially locked transition zone.

Because intraplate deformation rates are usually considerably lower than those in plate boundary zones, GPS will prove to be extremely important in measuring intraplate deformation. One strategy for obtaining strain estimates without waiting for long periods of time is to use GPS to resurvey existing geodetic networks. Liu et al (1992) resurveyed a triangulation network in the New Madrid seismic zone and found shear strain (significant at the 95% confidence level) to have accumulated during the last 35 years. Although errors in the early triangulation observations dominate the error budget, the fact that the orientation of the maximum shear is consistent with the local geology and seismicity, and that similar shear strains were obtained in two spatially distinct subnetworks, together suggest that the data have recorded true crustal strain. Repeated GPS observations over a broader region are not inconsistent with the Liu et al (1992) findings (Weber 1995), although they do suggest a lower average rate of deformation.

PLATE MOTIONS AND PLATE BOUNDARY DEFORMATION

Plate motion models based entirely on GPS data, which are dominantly from permanent GPS receivers at IGS sites, are beginning to appear (Figure 5). Argus & Heflin (1995) estimated the motion of six major plates (Pacific, North America, Eurasia, Australia, Africa, and South America) using IGS data for 43 globally distributed stations. The measured angular velocities agree with the NUVEL-1A (DeMets et al 1990, 1994) model within uncertainties for all plate
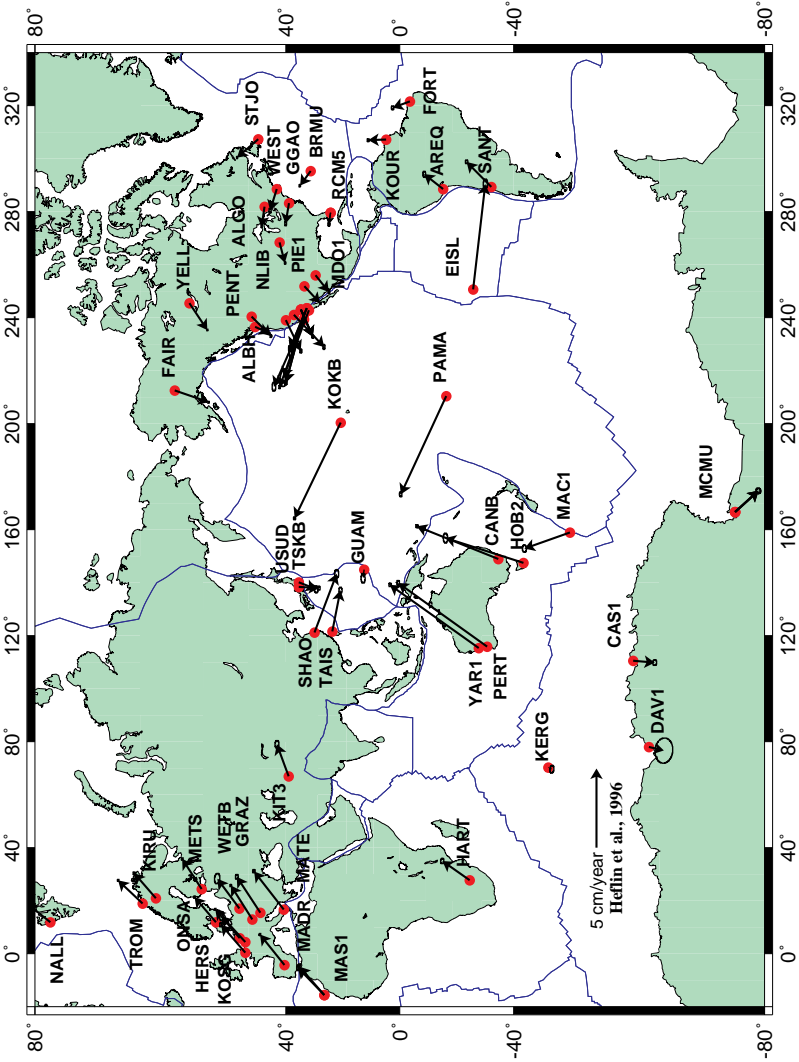
Figure 5 Horizontal velocities of permanent GPS sites of the International GPS Service for Geodynamics (IGS) network. The reference frame is ITRF94. Sites with the smallest error ellipses became operational in 1991 and have a time span of 5 years. The mean time span is 3 years. Figure courtesy of Michael Heflin, Jet Propulsion Lab. (see Argus & Heflin 1995).
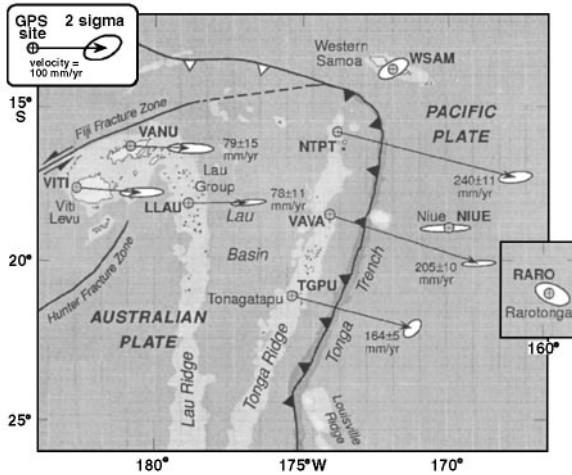
Figure 6   Velocities of sites in the Tonga arc and Lau basin in a Pacific-plate fixed-reference frame based on GPS data collected between 1990 and 1992. Error ellipses represent 2σ (86%) confidence intervals. After Bevis et al (1995).

pairs. These results are consistent with previous studies that have shown that the relative motion of plate interiors does not change measurably over time scales of years to millions of years. Larson & Freymueller (1995) used three years of IGS data from seven sites to estimate the motion of the Australian, Pacific, and Antarctic plates. Their study represents the first geodetic determination of Antarctic plate motion. The estimated rates agree with the NUVEL no-net-rotation model of absolute plate motion to within error measurements.

Although agreement with plate motion models such as NUVEL is confirming both of the plate models and the geodetically derived velocities, it is not possible simultaneously to test geologic models and use those same models to validate geodetic results. At this date it is safe to conclude that, assuming appropriate care has been given to maintaining a stable reference frame, GPS results provide accurate crustal motions, so that it is now possible to focus on the differences between geologic models and geodetic results. Because the rates of crustal deformation are generally slow, time is required before results are sufficiently robust to force modifications of existing models. For this reason, the greatest short term impact has been (or will be) made in plate boundary regions such as the Phillipine Sea plate and the Lau Basin, which are characterized by diffuse back arc spreading, so that the rates of plate motion are not well constrained by sea floor magnetic anomalies.

Rapid convergence between the Pacific and Australian plates at the Tonga Trench has been observed by Bevis et al (1995). The rate of motion between

three sites in Fiji, presumed to be on the Australian plate, and three sites on the Pacific plate were found to be in excellent agreement with NUVEL-1A predictions. Three stations on the Tonga Ridge, across the Lau Basin, moved away from the Australian plate at rates increasing from 91 ± 4 mm/year in the south to 159 ± 10 mm/year in northern Tonga (Figure 6). The data imply back-arc opening of the Lau Basin as the Tonga Ridge rotates clockwise at $\sim 7°$/million years about a pole near the southern end of the Lau Basin. Bevis et al (1995) suggested that the unusually high rates of mantle seismicity beneath the Tonga Trench may be associated with the very rapid rate of subduction and back arc spreading.

Taylor et al (1995) found that the convergence rate between the southern New Hebrides and the Australian plate is faster (103 ± 5 mm/year to 109 ± 10 mm/year) than the expected rate of Australian-Pacific convergence (79–86 mm/year in this region). On the other hand, in the central New Hebrides the observed relative motion of 42 ± 2 mm/year is significantly less than that expected from rigid plate motion. Taylor et al (1995) attribute the faster than expected rate in the southern New Hebrides to back arc spreading in the south Fiji basin. The slower than expected rate in the central New Hebrides is attributed to the impinging of the D'Entrecasteaux Ridge on the subduction zone. This results in eastward motion of the New Hebrides with respect to the Pacific plate, compression in the eastern part of the arc and strike-slip boundaries at either end of the indenting D'Entrecasteaux Ridge, which is consistent with earthquake focal mechanisms in the area.

Noomen et al (1996) employed a combination of SLR (1983–1992) and GPS surveys (1989 and 1992) to determine the motions of 19 sites in the Mediterranean region from southern France to eastern Turkey. They found the Arabian plate, including a station in eastern Turkey, to be moving northward with respect to Eurasia at a rate of ~ 20 mm/year. Stations in central Turkey (Anatolia) moved westward at a rate of slightly more than 20 mm/year with respect to the Eurasian plate. Four stations in the Hellenic arc moved southwest at a rate of 29 mm/year with respect to Eurasia. Using data from a more extensive GPS network, Oral et al (1995) concluded that Turkey south of the North Anatolian fault moves as a coherent microplate with a pole of rotation located north of the Sinai peninsula. The SLR measurements suggest that southern Greece and the Agean act as part of this microplate. Stations north of the North Anatolian fault exhibit much lower velocities with respect to the Eurasian plate, which is consistent with ~ 25 mm/year slip on the North Anatolian fault. A dense network across the North Anatolian fault shows localized deformation with maximum shear oriented E-W south of the Black Sea, whereas farther west, in the eastern Marmara Sea region, the strain is more distributed and the maximum shear is oriented WSW-ENE (Straub & Kahle 1995). Eastern

Turkey displays a complex pattern of oblique right-lateral convergence between the Arabian and Eurasia/Anatolia plates (Oral et al 1995).

Foulger et al (1992) and Heki et al (1993) reported on results from two GPS surveys in 1987 and 1990, 10 years after a major rifting episode on the neovolcanic zone in northeast Iceland. Rifting occurred during a series of intrusions and eruptions between 1975 and 1981, with a cumulative extension of 8 m across the rift system. Displacements of the GPS sites show that extension across a zone extending at least 100 km from the rift axis occurred roughly one decade after the rifting event. Heki et al (1993) modeled the motions with a two-dimensional elastic plate overlying a Newtonian viscous fluid. Sudden rifting events at the boundary of the model leads to the diffusion of strain (and stress) into the elastic plate. Using the measured opening across the rift zone as input, Heki et al (1993) found the best fit to the observations with a stress diffusivity of 10 m^2/s. Assuming the thickness of the elastic plate and underlying viscous channel is consistent with magnetotelluric results leads to a viscosity of 0.3 to 2.0×10^{18} Pascal-seconds. The vertical displacements do not correlate well with predictions of the Elsasser model, which is attributed to low precision in the GPS height determinations.

VOLCANO DEFORMATION

GPS holds great promise for the study of volcano deformation, which can be both episodic and rapid. Measurable deformation precedes some eruptions, which suggests the utility of GPS measurements in predicting volcanic hazards. Indeed, some dramatic GPS data have already been obtained related to volcanic processes.

A remarkable set of data was recorded prior to and during a submarine eruption off the coast of the Izu Peninsula in Japan (Shimada et al 1990; Fujinawa et al 1991). A seismic swarm, which began in late May 1989, intensified on July 4, 1989. A M5.5 event occurred on July 9, a harmonic tremor was recorded on July 11–12, and on July 13 there was dramatic doming of the sea surface and the onset of a phreatomagmatic eruption. A pair of GPS stations, one located on the Izu Peninsula and the other on Hatsushima Island, spanned the zone of seismicity. Although the GPS data were quite limited by today's standards, consisting of 4 h of data from 4 satellites per day, 14.5 cm of extension was ultimately recorded between the stations. Most importantly, the GPS data recorded clear changes on July 5 and 6, several days before the onset of harmonic tremor and a week prior to visible evidence of the eruption at the sea surface. The eruption itself was not accompanied by measurable deformation.

In addition to the GPS measurements, tilt, borehole strain, terrestrial EDM, and leveling data were also collected. Okada & Yamamoto (1991) used all the available data to develop a time-dependent kinematic model of the source

process. The model includes a deep dike-like source accompanying the May 1989 swarm, the M5.5 earthquake source, and the main dike that ultimately fed the eruption. The main dike was inferred to have been located at a depth of 7–5 km in early July, but grew to within 1 km of the sea floor by July 4, ultimately widening to well over a meter in width prior to the eruption. Okada & Yamamoto (1991) interpreted the lack of deformation accompanying the eruption to indicate that the magma intruded shallow compliant sediments, forming a sill prior to the eruption. Remarkably, bathymetric surveys showed a flat sea floor on July 9, but a survey on July 13, "minutes" before a phreatomagmatic eruption, shows a 25-m high by 300-m diameter knoll.

Rapid quasi-steady motions have been mapped on Kilauea volcano, Hawaii, using GPS (Owen et al 1995). The south flank of Kilauea, the area south of Kilauea's two rift zones, has generated large earthquakes including a M7.2 event in 1975. These quakes occurred on a buried subhorizontal fault (with the upper plate moving seaward), near the base of the volcanic pile at the contact with the ancient sea floor. GPS data collected between 1990 and 1993 show that the region north of the rift zones was not actively deforming, while the central south flank displaced seaward at rates of up to 10 cm/year (Figure 7). The extraordinarily high strain rates across the rift zones cannot be explained by aseismic slip on the decollement alone. Dilation of the rift zones below 3–4 km is required to decouple the south flank across the rift zones. Owen et al (1995) modeled the data with elastic dislocations representing the decollement and the rift zones. The GPS-derived horizontal motions require the basal fault to be slipping at a rate of at least 150 mm/year. Opening of the deep rift zone was inferred to have taken place at a comparable rate.

GLACIAL ISOSTATIC ADJUSTMENT AND SEA LEVEL CHANGE

GPS is also playing an important role in the determination of present-day sea-level change. Tide gauges record the level of the sea surface with respect to land, which may or may not be moving vertically. Accurate measurement of vertical displacement rates at tide gauge stations are thus needed to correct apparent sea-level records for crustal deformation. Vertical crustal motions can arise due to tectonic processes, groundwater and oil withdrawal, and ongoing isostatic adjustment in response to late Pleistocene deglaciation. The latter effect can be significant even far from the ancient ice sheets (e.g. Mitrovica & Davis 1995).

The Fennoscandian region has the longest tide gauge records in the world, but because of the large glacial isostatic adjustment (GIA) signal, it has not been possible to utilize these data for estimating present-day sea-level variations (e.g. Douglas 1991). Several GPS projects, including BIFROST (Baseline Inferences for Fennoscandian Rebound Observations, Sea Level, and Tectonics)
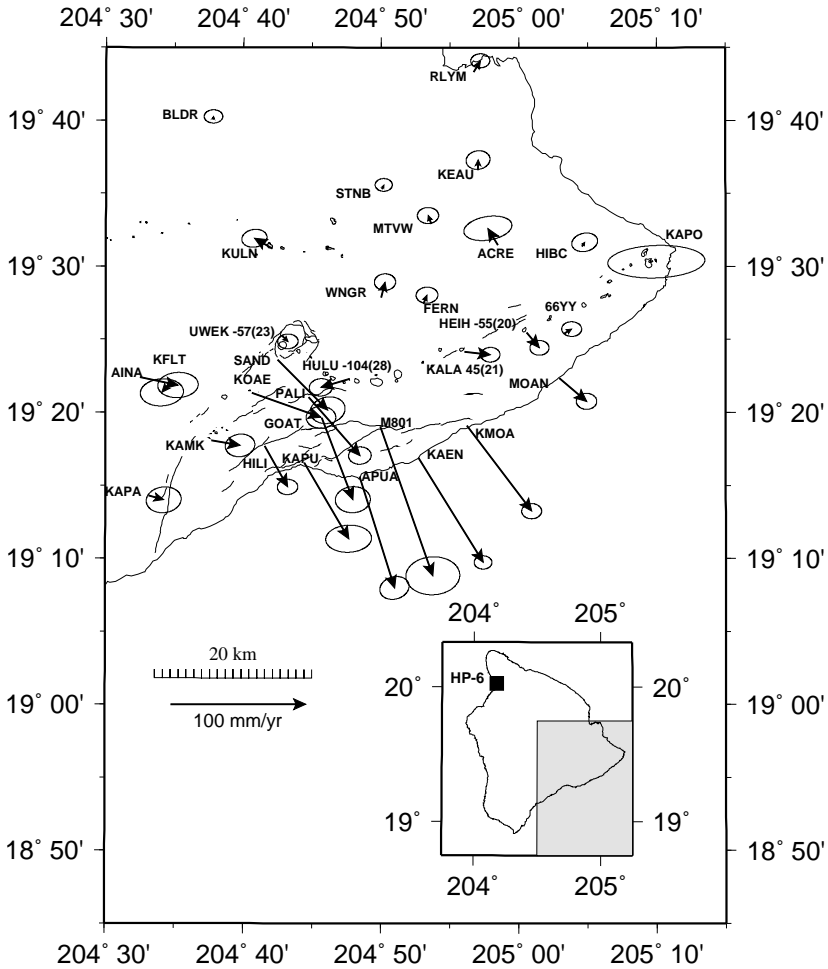
Figure 7   Average horizontal velocities on Kilauea volcano for the time interval 1990–1993. Velocities are shown relative to station HP-6 on the northwest side of the island of Hawaii. Error ellipses represent 95% confidence intervals. After Owen et al (1995).

(BIFROST Project 1996), which involves permanent GPS networks in Sweden and Finland, and the Baltic Sea Level Project (Pan & Sjöberg 1993), have the goal of correcting Fennoscandian tide gauges for GIA.

Another approach to estimating present-day sea-level change has been to use GPS to measure elastic deformations resulting from changes in the mass of glaciers and ice sheets (e.g. James & Ivins 1995; Wahr et al 1995). An increase in ice mass causes GPS sites on bedrock adjacent to the ice sheet

to subside, whereas a decrease in ice mass causes adjacent sites to rebound. For example, Sauber et al (1995) measured vertical crustal motions of up to 17 cm associated with the surging Bering Glacier. The difficulty is that the present rate of uplift results from a combination of a viscoelastic response to Pleistocene deglaciation as well as to the elastic response associated with ongoing changes in ice mass. Wahr et al (1995) suggested that a combination of precise gravity and GPS measurements can distinguish between these effects.

The Earth's three-dimensional response to variations in loading depends on both the ice-load history and the Earth's viscosity structure. Thus observations of GIA can be used to infer mantle viscosity and provide important information for models of mantle dynamics. The primary data set for observing the GIA response has been the global database of historic relative sea-level (RSL) curves (e.g. Tushingham & Peltier 1992). Inferences of mantle viscosity based on relative sea level and other data, however, continue to vary by an order of magnitude or more at all depths (e.g. Fjeldskaar & Cathles 1991; Tushingham & Peltier 1992). There are a number of possible causes for these discrepancies, including errors in deglaciation history, lack of assessment of resolving power and uncertainty (e.g. Mitrovica 1996), and lateral heterogeneity in mantle strength (e.g. Manga & O'Connell 1995). Finally, the uncertainty associated with much of the global database of RSL curves is difficult to establish. Curves obtained from the same region are often inconsistent, and in some cases uncertainties are so large that the data cannot be used to discern significant differences between Earth models. Furthermore, there is an inherent weakness associated with sea-level data sets: Observations are available only along shorelines, which provide sparse coverage.

GPS-derived determinations of deformation, particularly uplift, in areas of ongoing postglacial rebound will thus add invaluable data for testing models of mantle viscosity and ice-load history. The first significant vertical deformation rates to be determined by GPS have only recently become available (BIFROST Project 1996). Figure 8 shows GPS estimates of vertical motion in Fennoscandia obtained from 2.5 years of observations. As three-dimensional crustal velocity estimates obtained from this continuing project become more accurate, they will be used to refine models of mantle viscosity and ice history.

Uncertainties in mantle viscosity and ice history result in errors in predicted rates of GIA used to correct tide gauge data for vertical land motions. For example, anomalous GIA-corrected sea-level rates from tide gauges have been found on the east coast of North America (e.g. Douglas 1991), with the anomaly reaching a peak of ∼1 mm/year in the Chesapeake Bay area. Davis & Mitrovica (1996) demonstrated that this anomaly can be eliminated by a simple modification to the viscosity model used to calculate the GIA corrections. Ongoing GPS observations in the Chesapeake Bay area (S Nerem, personal communication)
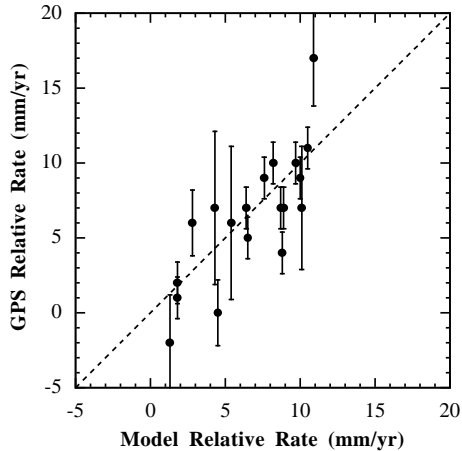
Figure 8 Comparison of observed and predicted model values for the vertical component of baseline-vector rates, from BIFROST Project (1996). The predictions are based on the spectral theory presented by Mitrovica et al (1994) and use realistic models for the viscoelastic structure of the Earth and the ice history.

will provide an important test of the predicted rates of postglacial rebound and the inferred mantle viscosity structure.

PERMANENT GPS NETWORKS

Permanent or continuous GPS networks, meaning a network of GPS receivers that are left in place for a long period, are not new. Permanent networks like CIGNET and the IGS network (e.g. Blewitt 1993) have proven their utility to the geodetic community for orbit determination and have also been used for plate tectonic studies (Larson & Freymueller 1995; Argus & Heflin 1995). As the price of GPS receivers has decreased, investigators have recently turned to regional permanent networks for geophysical studies. Shimada & Bock (1992) reported some of the earliest results from a permanent GPS network: 17 months of data from a 10-station array in the Kanto-Tokai (Tokyo) area of Japan. More recently, the BIFROST Project (1996) has measured postglacial uplift with a 21-site permanent GPS network in Sweden.

In practice, continuous GPS data is usually processed to yield one estimate of site position per day, although more frequent solutions (e.g. Figure 4) can be obtained. With these data, it is possible to study a wide range of transient deformation processes in tectonic and volcanic regions that are not possible with conventional (often annual) GPS field campaigns. Under the right conditions, daily position determinations may yield more accurate estimates of average

deformation rates than would periodic campaign measurements. What are the "right conditions"? Simply put, the right conditions are such that the errors in the position estimates "average out" over useful scales of space, time, or both. The efficiency with which the errors average out will be diminished if the errors are spatially or temporally coherent (e.g. Johnson & Agnew 1995).

Many of the error sources discussed previously may be spatially or temporally coherent. Atmospheric mapping function errors, precipitation, snow accumulation, multipath and antenna coupling (both of which may depend to some degree on environmental conditions), antenna phase center variations, and atmospheric pressure loading all might be expected to have some spatial and temporal coherence. Local surficial processes may lead to temporally correlated random motions of geodetic monuments. Langbein et al (1995) tested deeply anchored monuments that provide better coupling to the crust and hence improve their long-term stability.

Without doubt, the most ambitious continuous GPS network is the Japanese national network (Figure 9). At the time of this writing, there are 610 permanent GPS stations operated by the Geographical Survey Institute (GSI) of Japan (Miyazaki et al 1996). This network represents the merging of the nationwide GPS Regional Array for Precise Surveying (GRAPES) and the Continuous Strain Monitoring System (COSMOS), located in the Kanto-Tokai areas around metropolitan Tokyo. Station spacing throughout the country is roughly 30 km, but around Tokyo the stations are more concentrated. A number of interesting results have already been obtained from the GSI network, including coseismic displacements associated with three M7 and greater earthquakes, as discussed in a previous section. Strain transients following the M7.5 1994 Sanriku-Haruka-Oki earthquake (Figure 4) and associated with volcanic processes off the Izu peninsula have been recorded. Preliminary results have been obtained showing interseismic deformation over the entire country of Japan for the past year. These data should prove to be invaluable in determining the spatial distribution of strain accumulation and the location of the elusive Eurasian–North America (or Eurasian-Okhotsk) plate boundary, as well as in obtaining an improved understanding of the physics of subduction zones.

Permanent GPS networks for the study of crustal deformation have been developed in southern and northern California and the northern Basin and Range. The Southern California Integrated GPS Network (SCIGN) presently consists of 40 operational stations. Thirty new stations are planned, and funding has been requested for an additional 45 stations. The Basin and Range permanent GPS network, currently being implemented, extends from the Sierra Nevada to the Wasatch Front and is intended to measure the distribution of deformation in this region.

In northern California, the Bay Area Regional Deformation (BARD) GPS network consists of 25 permanent and semipermanent stations and should
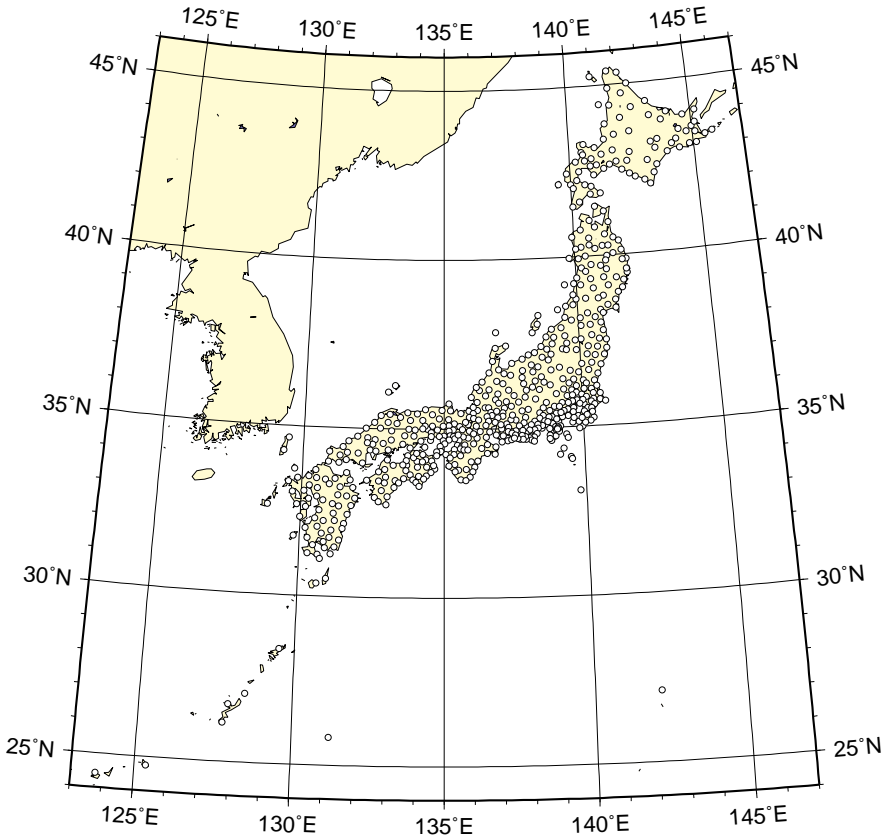
Figure 9   Permanent GPS network in Japan, operated by the Geographical Survey Institute of Japan. Figure courtesy of Takeshi Sagiya (GSI).

expand to at least 40 receivers in 1997. King et al (1995) investigated three years of BARD data spanning the Hayward fault, to determine the error characteristics of the data. They found that the data are essentially uncorrelated at lags longer than 25 days and are only weakly correlated for lags shorter than 10 days. Within the frequency range studied (0.01–0.5 cycles per day for the daily sampled data), the power spectra are only mildly enhanced at low frequencies.

THE FUTURE

Some present trends seem likely to have a large impact on the future of GPS geodesy. The price of GPS receivers is decreasing, promoting the growth of

permanent, dedicated regional networks for geophysical studies. Data collected for nonresearch applications (e.g. aircraft and ship navigation, regional differential GPS networks) are, and will increasingly become, available for research uses. Whereas in the past, permanent networks sacrificed spatial for temporal resolution, the increased density of some GPS networks (e.g. in Japan and California) will provide unprecedented spatial and temporal sampling of crustal deformation. Enhanced spatial coverage is vital for detecting coherent tectonic signals.

A number of error sources that previously had not been considered in GPS studies are now receiving serious consideration. The proliferation of permanent GPS systems provides as much data as any researcher can handle, from a wide variety of locations, environments, and physical installations. Hypotheses concerning the "repeatability" of parameter estimates may be rigorously tested, and the time- and space-dependence of parameter variations may be carefully examined. This wealth of data is a two-edged sword, for the groups whose primary task it is to process these data operationally can be strained simply to keep up with the flow of data.

Newly collected GPS data should provide a tremendous improvement in our understanding of postseismic deformation. Increased spatial coverage will have a profound impact on regional GPS studies. The number of sites will increase from a few per plate, in many places, to the density needed to map the strain-rate distribution and to associate features in the deformation field with specific tectonic structures. The precision, greatly increased spatial coverage, and frequent sampling provided by current and future GPS networks will reveal the detailed space-time pattern of crustal deformation. These will in turn lead to substantial insights into the rheology of the crust and mantle and will allow for time-dependent inversions for fault-slip distribution and the evolving geometry of magma bodies.

Visit the *Annual Reviews home page* at
http://www.annurev.org.

Literature Cited

Aki K, Richards PG. 1980. *Quantitative Seismology: Theory and Methods.* San Francisco: Freeman. 932 pp.

Argus DF, Heflin MB. 1995. Plate motion and crustal deformation estimated with geodetic data from the Global Positioning System. *Geophys. Res. Lett.* 22:1973–76

Árnadóttir T, Beavan J, Pearson C. 1995. De-

formation associated with the 18 June, 1994, Arthur's Pass earthquake, New Zealand. *NZ. J. Geol. Geophys.* 38:553–58

Árnadóttir T, Segall P. 1994. The 1989 Loma Prieta earthquake imaged from inversion of geodetic data. *J. Geophys. Res.* 99(B11): 21835–55

Beavan J. 1993. Surface deformation due to the M_w 7.8 Guam earthquake of August 8, 1993. *Eos, Trans. Am. Geophys. Union* 74:183 (Abstr.)

Bennett RA, Reilinger RE, Rodi W, Li Y, Toksöz MN, Hadnut K. 1995. Coseismic fault slip associated with the 1992 M_w 6.1 Joshua Tree, California, earthquake: implications for the Joshua Tree-Landers earthquake sequence. *J. Geophys. Res.* 100(B4):6443–61

Bennett RA, Rodi W, Reilinger RE. 1996. Global Positioning System constraints on fault slip rates in southern California and northern Baja, Mexico. *J. Geophys. Res.* 101(B10):21943–60

Beutler G, Brockmann E, Hugentobler U, Mervart L, Rotacher M, Weber R. 1996. Combining consecutive short arcs into long arcs for precise and efficient GPS orbit determination. *J. Geodesy* 70:287–99

Beutler G, Morgan P, Neilan RE. 1993. Geodynamics: tracking satellites to monitoring global change. *GPS World* 4(2):40–42, 44, 46

Bevis M, Taylor FW, Schutz BE, Recy J, Isacks BL, et al. 1995. Geodetic observations of very rapid convergence and back-arc extension at the Tonga arc. *Nature* 374(6519):249–51

BIFROST Project Members. 1996. GPS measurements to constrain geodynamic processes in Fennoscandia. *Eos, Trans. Am. Geophys. Union*. 77(E07):337 and 341

Blewitt G. 1993. Advances in Global Positioning System technology for geodynamics investigations: 1978–1992. In *Contrib. Space Geodesy Geodyn.: Technol. Geodyn.*, *Geodyn. Ser.*, ed. DE Smith, DL Turcotte, 25: 195–213. Washington, DC: Am. Geophys. Union. 213 pp.

Blewitt G, Heflin MB, Hurst KJ, Jefferson DC, Webb FH, Zumberge JF. 1993. Absolute far-field displacements from the 28 June 1992 Landers earthquake sequence. *Nature* 361(6410):340–42

Bock Y, Agnew DC, Fang P, Genrich JF, Hager BH, et al. 1993. Detection of crustal deformation from the Landers earthquake sequence using continuous geodetic measurements. *Nature* 361(6410):337–40

Bürgmann R, Segall P, Lisowski M, Svarc JP. 1996. Post-seismic strain following the 1989 Loma Prieta earthquake from repeated GPS and leveling measurements. *J. Geophys. Res.* In press

Cohee BP, Beroza GC. 1994. A comparison of two methods for earthquake source inversion using strong motion seismograms. *Ann. Geofis.* 37(6):1515–38

Davis JL, Elgered G, Niell AE, Kuehn CE. 1993. Ground-based measurement of gradients in the "wet" radio refractivity of air. *Radio Sci.* 28:1003–18

Davis JL, Herring TA, Shapiro II. 1991. Effects of atmospheric modeling errors on determinations of baseline vectors from very long baseline interferometry. *J. Geophys. Res.* 96:643–50

Davis JL, Herring TA, Shapiro II, Rogers AEE, Elgered G. 1985. Geodesy by radio interferometry: effects of atmospheric modeling errors on estimates of baseline length. *Radio Sci.* 20:1593–1607

Davis JL, Mitrovica JX. 1996. Glacial isostatic adjustment and the anomalous tide gauge record of eastern North America. *Nature* 379:331–33

DeMets C, Gordon RG, Argus DF, Stein S. 1990. Current plate motions. *Geophys. J. Int.* 101:425–78

DeMets C, Gordon RG, Argus DF, Stein S. 1994. Effect of recent revisions to the geomagnetic reversal time scale on estimates of current plate motions. *Geophys. Res. Lett.* 21:2191–94

Dixon TH. 1991. An introduction to the Global Positioning System and some geological applications. *Rev. Geophys.* 29:249–76

Donnellan AB, Hager H, King RW. 1993. Discrepancy between geologic and geodetic deformation rates in the Ventura basin. *Nature* 366:333–36

Douglas BC. 1991. Global sea level rise. *J. Geophys. Res.* 96:6981–92

Dragert H, Hyndman RD. 1995. Continuous GPS monitoring of elastic strain in the northern Cascadia subduction zone. *Geophys. Res. Lett.* 22(7)755–58

Du YJ, Segall P, Gao HJ. 1994. Dislocations in inhomogeneous media via a moduli perturbation approach: general formulation and two-dimensional solutions. *J. Geophys. Res.* 99:3767–79

Dvorak J. 1994. An earthquake cycle along the south flank of Kilauea Volcano, Hawaii. *J. Geophys. Res.* 99(B5):9533–41

Elgered G, Davis JL, Herring TA, Shapiro II. 1991. Geodesy by radio interferometry: Water Vapor Radiometry for estimation of the wet delay. *J. Geophys. Res.* 96:6541–55

Elósegui P, Davis JL, Jaldehag RTK, Johansson JM, Niell AE, Shapiro II. 1995. Geodesy using the Global Positioning System: the effect of signal scattering on estimates of site position. *J. Geophys. Res.* 100:9921–34

Elósegui P, Davis JL, Johansson JM, Shapiro II. 1996. Detection of transient motions with the Global Positioning System. *J. Geophys. Res.* 101(11):11249–61

Feigl KL, Agnew DC, Bock Y, Dong D, Donnellan A, et al. 1993. Space geodetic measurement of crustal deformation in central and southern California, 1984–1992. *J. Geophys. Res.* 98(B12):1677–712

Feigl KL, King RW, Herring T, Rotacher M. 1991. A scheme for reducing the effect of selective availability on precise geodetic measurements from the Global Positioning System. *Geophys. Res. Lett.* 18:1289–92

Fjeldskaar W, Cathles L. 1991. Rheology of mantle and lithosphere inferred from postglacial uplift in Fennoscandia. In *Glacial Isostasy, Sea-Level, and Mantle Rheology*, ed. R Sabadini, K Lambeck, E Boschi, pp. 1–19. Dordrecht: Kluwer

Fliegel HF, Gallini TE, Swift ER. 1992. Global Positioning System radiation force model for geodetic applications. *J. Geophys. Res.* 97:559–68

Foulger GR, Jahn CH, Seeber G, Einarsson P, Julian BR, Heki K. 1992. Post-rifting stress-relaxation at the divergent plate boundary in NE Iceland. *Nature* 358:488–90

Freymueller J, King NE, Segall P. 1994. The co-seismic slip distribution of the Landers earthquake. *Bull. Seismol. Soc. Am.* 84(3):646–59

Fujinawa Y, Shimada S, Ohmi S, Sekiguchi S, Eguchi T, Okada Y. 1991. Fixed point GPS observation of crustal movement associated with the 1989 seismic swarm and submarine volcanic activities off Ito, central Japan. *J. Phys. Earth* 39:141–53

Genrich JF, Bock Y. 1992. Rapid resolution of crustal motion at short ranges with the Global Positioning System. *J. Geophys. Res.* 97:3261–69

Hager BH, King RW, Murray MH. 1991. Measurement of crustal deformation using the Global Positioning System. *Annu. Rev. Earth Planet. Sci.* 19:351–82

Heflin MB, Bertiger WI, Blewitt G, Freedman AP, Hurst KJ, et al. 1992. Global geodesy using GPS without fiducial sites. *Geophys. Res. Lett.* 19:131–34

Heki K, Foulger GR, Julian BR, Jahn CH. 1993. Plate dynamics near divergent boundaries: geophysical implications of postrifting crustal deformation in NE Iceland. *J. Geophys. Res.* 98(B8):14279–97

Hofmann-Wellenhof B, Lichtenegger H, Collins J. 1994. *GPS Theory and Practice.* New York: Springer-Verlag. 3rd ed.

Hudnut KW, Bock Y, Cline M, Fang P, Feng Y, et al. 1994. Co-seismic displacements of the 1992 Landers earthquake sequence. *Bull. Seismol. Soc. Am.* 84:625–45

Hudnut KW, Shen Z, Murray M, McClusky S, King R, et al. 1996. Co-seismic displacements of the 1994 Northridge, California, earthquake. *Bull. Seismol. Soc. Am.* 86(1B):S19–36

Jaldehag RTK. 1995. Space geodetic techniques: an experimental and theoretical study of antenna related error sources. *Tech. Rep. 276.* Goteborg, Sweden: Chalmers Univ. Technol.

Jaldehag RTK, Johansson JM, Ronnang BO, Elósegui P, Davis JL, Shapiro II. 1996. Geodesy using the Swedish permanent GPS network: effects of snow accumulation on estimates of site positions. *Geophys. Res. Lett.* 23:1601–4

James TS, Ivins ER. 1995. Present-day Antarctic ice changes and crustal motion. *Geophys. Res. Lett.* 22:973–76

Johansson JM, Elgered G, Davis JL. 1993. Wet path delay algorithms for use with microwave radiometer data. In *Contrib. Space Geodesy Geodyn.: Technol.*, *Geodyn. Ser.*, ed. DE Smith, DL Turcotte, 25:81–98. Washington, DC: Am. Geophys. Union

Johnson HO, Agnew DC, Hudnut K. 1994. Extremal bounds on earthquake movement from geodetic data; application to the Landers earthquake. *Bull. Seismol. Soc. Am.* 84(3):660–67

Johnson HO, Agnew DC. 1995. Monument motion and measurements of crustal velocities. *Geophys. Res. Lett.* 22:2905–8

King NE, Svarc JL, Fogleman EB, Gross WK, Clark KW, et al. 1995. Continuous GPS observations across the Hayward Fault, California, 1991–1994. *J. Geophys. Res.* 100(B10):271–83

Krauss JD. 1988. *Antennas.* New York: McGraw-Hill. 892 pp. 2nd ed.

Kuehn CE, Elgered G, Johansson JM, Clark TA, Rönnäng BO. 1993. A microwave radiometer comparison and its implications for the accuracy of wet delays. In *Contrib. Space Geodesy Geodyn.: Technol.*, *Geodyn. Ser.*, ed. DE Smith, DL Turcotte. 25:99–114. Washington, DC: Am. Geophys. Union

Langbein J, Wyatt F, Johnson H, Hamann D, Zimmer P. 1995. Improved stability of a deeply anchored geodetic monument for deformation monitoring. *Geophys. Res. J.* 22(24):3533–36

Larsen S, Reilinger R, Neugebauer H, Strange W. 1992. Global Positioning System measurements of deformations associated with the 1987 Superstition Hills earthquake. *J. Geophys. Res.* 97(4):4885–902

Larson KM. 1993. Application of the Global Positioning System to crustal deformation

measurements. 3. Results from the southern California borderlands. *J. Geophys. Res.* 98(B12):1713–26

Larson KM, Agnew DC. 1991. Application of the Global Positioning System to crustal deformation measurements. 1. Precision and accuracy. *J. Geophys. Res.* 96(B10):16547–65

Larson KM, Freymueller J. 1995. Relative motions of the Australian, Pacific and Antarctic plates estimated by the Global Positioning System. *Geophys. Res. Lett.* 22(1):37–40

Larson KM, Lisowski M. 1994. Strain accumulation in the Shumagin Islands: results of initial GPS measurements. *Geophys. Res. Lett.* 21(6):489–92

Larson KM, Webb FH, Agnew DC. 1991. Application of the Global Positioning System to crustal deformation measurements. 2. The influence of errors in orbit determination networks. *J. Geophys. Res.* 96(B10):16567–84

Leick A. 1995. *GPS Satellite Surveying.* New York: Wiley & Sons. 560 pp.

Lisowski M, Prescott WH, Savaga JC, Johnstone MJS. 1990. Geodetic estimate of coseismic slip during the 1989 Loma Prieta, California, earthquake. *Geophys. Res. Lett.* 17(9):1437–40

Liu LB, Zoback MD, Segall P. 1992. Rapid intraplate strain accumulation in the New Madrid seismic zone. *Science* 257:1666–69

Lu G, Lachapelle G. 1992. Statistical quality control for kinematic GPS positioning. *Manuscr. Geod.* 17:270–81

Lundgren PR, Wolf SK, Protti M, Hurst KJ. 1993. GPS measurements of crustal deformations associated with the 22 April 1991, Valle de la Estrella, Costa Rica earthquake. *Geophys. Res. Lett.* 20(5):407–10

MacMillan DS. 1995. Atmospheric gradients from very long baseline interferometry. *Geophys. Res. Lett.* 22:1041–44

Manga M, O'Connell RJ. 1995. The tectosphere and postglacial rebound. *Geophys. Res. Lett.* 22:1949–52

Massonet D, Feigl KL, Vadon H, Rossi M. 1996. Coseismic deformation field of the $M = 6.7$ Northridge, California earthquake of January 17, 1994 recorded by two radar satellites using interferometry. *Geophys. Res. Lett.* 23:969–72

Matthews MV, Segall P. 1993. Statistical inversion of crustal deformation data and estimation of the depth distribution of slip in the 1906 earthquake. *J. Geophys. Res.* 98:12153–63

Melbourne T, Carmichael I, DeMets C, Hudnut K, Sanchez O, et al. 1996. Shallow faulting and regional subsidence in the Mw 8.0 1995 Jalisco Subduction earthquake. *Geophys. Res. Lett.* (Submitted)

Merminod B, Rizos C. 1994. Optimisation of rapid static GPS surveys. *Manuscr. Geod.* 19:231–46

Mitrovica JX. 1996. Haskell (1935) revisited. *J. Geophys. Res.* 101:555–69

Mitrovica JX, Davis JL. 1995. Sea level change far from the Late Pleistocene ice sheets: implications for recent analyses of tide gauge records. *Geophys. Res. Lett.* 22:2529–32

Mitrovica JX, Davis JL, Shapiro II. 1994. A spectral formalism for computing three-dimensional deformations due to surface loads, 1. Theory. *J. Geophys. Res.* 99:7057–74

Miyazaki S, Tsuji H, Hatanaka Y, Abe Y, Yoshimura A, et al. 1996. Establishment of the nationwide GPS array (GRAPES) and its inital results on the crustal deformation of Japan. *Bull. Geogr. Surv. Inst.*(Jpn.) 42:27–41

Murray M, Marshall GA, Lisowski M, Stein RS. 1996. The 1992 $M = 7$ Cape Mendocino, California, Earthquake: coseismic deformation at the south end of the Cascadia megathrust. *J. Geophys. Res.* 101:17707–25

Niell AE. 1996. Global mapping functions for the atmospheric delay at radio wavelengths. *J. Geophys. Res.* 101:3227–46

Noomen R, Springer TA, Ambrosius BAC, Herzberger K, Kuijper DC, et al. 1996. Crustal deformations in the Mediterranean area computed from SLR and GPS observations. *J. Geodyn.* 21:73–96

Office of Science and Technology Policy. 1996. *US Global Positioning System Policy, Fact Sheet*. Washington, DC: Off. Sci. Technol. Policy

Okada Y, Yamamoto E. 1991. A dyke intrusion model for the 1989 seismovolcanic activity off Ito, central Japan. *J. Geophys. Res.* 96:10361–76

Oral MB, Reilinger RE, Toksoz MN, King RW, Barka AA, et al. 1995. Global Positioning System offers evidence of plate motions in the eastern Mediterranean. *Eos, Trans. Am. Geophys. Union* 76(2):9–11

Owen S, Segall P, Freymueller J, Miklius A, Denlinger R, et al. 1995. Rapid deformation of the south flank of Kilauea Volcano, Hawaii. *Science* 267:1328–32

Pan M, Sjöberg LE. 1993. Baltic Sea Level project with GPS. *Bull. Géod.* 67:51–59

Parkinson BW, Spilker JJ Jr, Axelrad P, Enge P, eds. 1996. *Global Positioning System: Theory and Applications.* Washington, DC: Am. Inst. Aeronaut. Astronaut. 2 Vol.

Rocken C, Johnson J, Nielan RE, Cerezo M, Jordan J, et al. 1991. The measurements of atmospheric water vapor: radiometer comparison and spatial variations. *IEEE Trans. Geosci. Remote Sens.* 29:3–8

Rocken C, Meertens C. 1991. Monitoring selective availability dither frequencies and their effect on GPS data. *Bull. Géod.* 65:162–69

Rocken C, Van Hove T, Johnson J, Solheim F, Ware R, et al. 1995. GPS/STORM—GPS sensing of atmospheric water vapor for meteorology. *J. Atmos. Ocean. Technol.* 12:468–78

Ruegg JC, Campos J, Armijo R, Barrientos S, Briole P, et al. 1996. The $M_w = 8.1$ Antofagasta (North Chile) earthquake of July 30, 1995: first results from teleseismic and geodetic data. *Geophys. Res. Lett.* 23:917–20

Santerre R. 1991. Impact of GPS satellite sky distribution. *Manuscr. Geod.* 16:28–53

Sauber J, Plafker G, Gipson J. 1995. Geodetic measurements used to estimate ice transfer during Bering Glacier surge. *Eos, Trans. Am. Geophys. Union* 76:289–90

Savage JC, Lisowski M, Svarc JL. 1994. Postseismic deformation following the 1989 ($M = 7.1$) Loma Prieta, California, earthquake. *J. Geophys. Res.* 99:13757–65

Savage JC, Svarc JL. 1997. Postseismic deformation associated with the 1992 $M_w = 7.3$ Landers earthquake, southern California. *J. Geophys. Res.* In press

Schupler BR, Allshouse RL, Clark TA. 1994. Signal characteristics of GPS user antennas. *Navigation* 41:277–95

Shen Z, Ge BX, Jackson DD, Potter D, Cline M, Sung L. 1996. Northridge earthquake ruptures based on the Global Positioning System measurements. *Bull. Seismol. Soc. Am.* 86(1B):37–48

Shen ZK, Jackson DD, Feng Y, Cline M, Kim M, et al. 1994. Postseismic deformation following the Landers earthquake, California, 28 June 1992. *Bull. Seismol. Soc. Am.* 84:780–91

Shimada S, Bock Y. 1992. Crustal deformation measurements in central Japan determined by a Global Positioning System fixed point network. *J. Geophys. Res.* 97:12437–55

Shimada S, Fujinawa Y, Sekiguchi S, Ohmi S, Eguchi T, Okada Y. 1990. Detection of a volcanic fracture in Japan using Global Positioning System measurements. *Nature* 343:631–33

Straub C, Kahle HG. 1995. Active crustal deformation in the Marmara Sea region, NW Anatolia, inferred from GPS measurements. *Geophys. Res. Lett.* 22:2533–36

Tabei T, Kato T, Catane JPL, Chachin T, Fujimori K, et al. 1996. Crustal deformation associated with the 1995 Hyogo-ken Nanbu earthquake, Japan, derived from GPS measurements. *J. Phys. Earth.* Special issue. In press

Taylor FW, Bevis MG, Kuang D, Schutz BE, Recy J, et al. 1995. Geodetic measurements of convergence at the New Hebrides island arc indicate arc fragmentation caused by an impinging aseismic ridge. *Geology* 23(11):1011–14

Tranquilla JM, Al-Rizzo HM. 1993. Theoretical and experimental evaluation of precise relative positioning during periods of snowfall precipitation using the Global Positioning System. *Manuscr. Geod.* 18:362–79

Tranquilla JM, Carr JP, Al-Rizzo HM. 1994. Analysis of a choke ring groundplane for multipath control in Global Positioning System (GPS) applications. *IEEE Trans. Antennas Propag.* 42:905–11

Tsuji H, Hatanaka Y, Sagiya T, Hashimoto M. 1995. Coseismic crustal deformation from the 1994 Hokkaido-Toho-Oki earthquake monitored by a nationwide continuous GPS array in Japan. *Geophys. Res. Lett.* 22(13):1669–72

Tushingham AM, Peltier WR. 1992. Validation of the ICE-3G model of Wurm-Wisconsin deglaciation using a global data base of relative sea level histories. *J. Geophys. Res.* 97:3285–304

vanDam TM, Blewitt G, Heflin MB. 1994. Atmospheric pressure loading effects on Global Positioning System coordinate determinations. *J. Geophys. Res.* 99:23939–50

Wahr J, DaZhong H, Trupin A. 1995. Predictions of vertical uplift caused by changing polar ice volumes on a viscoelastic Earth. *Geophys. Res. Lett.* 22:977–80

Wald DJ, Heaton TH. 1994. Spatial and temporal distribution of slip for the 1992 Landers, California, earthquake. *Bull. Seismol. Soc. Am.* 84(3):668–91

Wald DJ, Heaton TH, Hudnut KW. 1996. The slip history of the 1994 Northridge, California, earthquake determined from strong-motion, teleseismic, GPS, and leveling data. *Bull. Seismol. Soc. Am.* 86(1B):S49–70

Ware R, Rocken C, Solheim F, Van Hove T, Alber C, Johnson J. 1993. Pointed Water Vapor Radiometer corrections for accurate Global Positioning System surveying. *Geophys. Res. Lett.* 20:2635–38

Weber JC. 1995. *New Madrid seismic zone deformation from repeat Global Positioning System (GPS) surveys*. PhD thesis. Northwestern Univ., Evanston, Ill. 141 pp.

Williams C, Arnadottir T, Segall P. 1993. Coseismic deformation and dislocation models of the 1989 Loma Prieta earthquake derived from Global Positioning System measurements. *J. Geophys. Res.* 98:4567–78

Wu JT, Wu SC, Hajj GA, Bertiger WI, Lichten SM. 1993. Effects of antenna orientation on

GPS carrier phase. *Manuscr. Geod.* 18:91–98

Yoshida S, Koketsu K, Shibazaki B, Sagiya T, Kato T, Yoshida Y. 1996. Joint inversion of near and far-field waveforms and geodetic data for the rupture process of the 1995 Kobe earthquake. *J. Phys. Earth.* Special issue. In press

Yuan LL, Anthes RA, Ware RH, Rocken C, Bonner WD, et al. 1993. Sensing climate change using the global positioning system. *J. Geophys. Res.* 98:14925–37

Zumberge JF, Liu R, Neilan RE. 1995. *1994 Annual Rep., Int. GPS Serv. Geodyn., IGS Central Bur.*, Jet Propulsion Lab., Pasadena, CA